Analysis of Thermo-Optic Tunable Dispersion-Engineered Short-Wavelength-Pass Tapered-Fiber Filters

Sen-Yih Chou, Kuei-Chu Hsu, Nan-Kuang Chen, Shien-Kuei Liaw, Yu-Syun Chih, Yinchieh Lai, and Sien Chi

***Abstract*—Thermo-optic tunable short-wavelength-pass tapered-fiber filters based on fundamental-mode cutoff mechanism are realized experimentally and analyzed theoretically. The effects of material and waveguide dispersion are investigated and the optimal tapered fiber structures for attaining high-spectral cutoff slope and high-rejection efficiency are determined.**

***Index Terms*—Dispersion engineering, fiber filters, fiber optics, fiber tapering, fundamental-mode cutoff, thermo-optic.**

I. Introduction

STRONGER interaction of the optical evanescent field with the environment has been widely utilized in many fiber-based devices such as the fused-tapered-based fiber filters [1], [2], dispersion-engineering applications [3]–[5] and nanowire sensing applications [6], [7]. The dispersion-engineering techniques manipulate the dispersion characteristics of fiber waveguides to alter the optical properties of fiber devices. Previously, we had developed cost-effective thermo-optic tunable short-wavelength-pass fiber filters [8]–[11] based on the fundamental-mode cutoff concept. We had also successfully demonstrated *S*-band erbium-doped fiber amplifiers and lasers by utilizing these fiber filters to extend the gain bandwidth of conventional Er-fibers toward *S*-band. Achieving high-performance *S*-band amplifiers and lasers critically depends on the high-cutoff slope and high-rejection efficiency of the tapered-fiber filters. Although in the literatures the theoretical modeling of tapered fibers had been widely developed [12]–[16], the fundamental-mode cutoff effects induced by dispersion-engineering techniques with fiber tapering have not been theoretically investigated yet. Our main objective here is thus to theoretically analyze the fundamental-mode cutoff effects and to determine the optimal tapered-fiber structures for achieving low-loss and high-cutoff efficiency. These results should be very crucial for applications such as high-gain low-noise *S*-band fiber amplifiers [9] and widely tunable *S*-band fiber lasers [10].

In the present work, we will present experimental characterization and theoretical simulation results on the studied thermo-optic tunable fused-tapered-fiber filters made by tapering standard single-mode fibers (SMF-28). The tapered fibers are immersed in Cargille liquids for implementing dispersion engineering through the control of material dispersion. The filter becomes cutoff at longer wavelengths due to the reducing refractive index of the Cargille liquids below the effective refractive index of the fiber waveguide. The propagation loss increases rapidly near the cutoff wavelength, and a sharp short-wavelength-pass optical filtering edge is achieved. To investigate these effects more deeply, the effective index (n_{eff}) and the mode field diameter (MFD) of the fundamental mode are calculated and carefully examined in order to understand what determines the filter performance. The numerical beam propagation method (BPM) is then adopted to theoretically simulate the cutoff phenomena and the temperature tuning characteristics of the whole device. Good agreement between the simulation and experimental results has been found. Since the filter performance is also significantly influenced by the whole waveguiding structure, the optimal parameters for the uniform taper diameter, uniform taper length, and taper transition length are investigated by the full BPM simulation for achieving best filter performance. From the simulated spectral responses and the effective dispersion curves, we find that the taper-waist diameter greatly affects the MFD, which in turn affects the final dispersion relation and the achievable cutoff slope. The taper length can also affect the cutoff slope, and the transition length has direct impacts on the insertion loss. The obtained theoretical results help us to determine the optimal device structures for fabricating efficient short-pass tapered-fiber filters which can be utilized in high performance *S*-band Er-fiber amplifiers and lasers.

Manuscript received May 09, 2008; revised August 10, 2008. First published April 17, 2009; current version published June 26, 2009.

S.-Y. Chou is with the Department of Photonics and Institute of Electro-Optical Engineering, National Chiao-Tung University, Hsinchu 300, Taiwan and also with the Center for Measurement Standards, Industrial Technology Research Institute, Hsinchu 300, Taiwan.

K.-C. Hsu is with the of Optics and Photonics, National Central University, Jhong-Li 320, Taiwan (e-mail:jessica.eo91g@nctu.edu.tw).

N.-K. Chen is with the Department of Electro-Optical Engineering, National United University, Miaoli, Taiwan 360, R.O.C., Optoelectronics Research Center, National United University, Miaoli, Taiwan 360, R.O.C.

S.-K. Liaw is with the Graduate Institute of Electro-Optical Engineering, National Taiwan University of Science and Technology, Taipei, Taiwan 106, R.O.C.

Y.-S. Chih and Y. Lai are with the Department of Photonics and Institute of Electro-Optical Engineering, National Chiao-Tung University, Hsinchu, Taiwan 300, R.O.C.

S. Chi is with the Department of Photonics and Institute of Electro-Optical Engineering, National Chiao-Tung University, Hsinchu, Taiwan 300, R.O.C. and also with the Department of Electro-Optical Engineering, Yuan Ze University, Chungli, Taiwan 320, R.O.C.

Color versions of one or more of the figures in this paper are available online at http://ieeexplore.ieee.org.

Digital Object Identifier 10.1109/JLT.2008.2005912

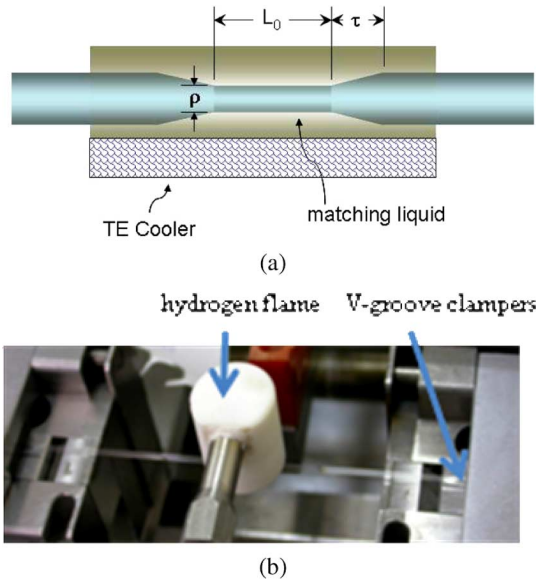

Fig. 1. (a) Diagram of a tapered-optical-fiber structure with a uniform waist. (b) Schematic diagram of the tapering station used to fabricate the tapered fibers.

II. Fabrication Process and Operation Principle

The high-cutoff efficiency of the studied short-pass fiber filters is obtained by locally modifying the material and waveguide dispersion within the uniform taper region. The schematic of the fused-tapered short-pass filter is shown in Fig. 1(a). One can describe the structure of a tapered-fiber filter by specifying the transition length (denoted as τ), the uniform waist length (denoted as L_0) and the waist diameter (denoted as ρ). It consists of a transition zone where the diameter is gradually reduced to ρ over a distance τ and then a uniform waist section with the length of L_0. The uniform waist section is immersed within suitable Cargille index-matching liquids. The optical properties of the used Cargille liquids can be summarized as follows. The refractive index $n_{\mathrm{D}} = 1.456$, thermo-optic coefficient $dn_{\mathrm{D}}/dT = -3.74 \times 10^{-4}/^{\circ}\mathrm{C}$, and optical transmittance is 88% at 1300 nm, and 80% at 1550 nm for 1-cm-long interaction length. The whole device is mounted on a thermoelectric (TE) cooler for temperature control. Those tapered-fiber filters are fabricated by a homemade tapering workstation comprising several modules for fiber pulling, heating, and scanning as illustrated in Fig. 1(b). A hydrogen flame head with high-accuracy flow control is set on a three axis stepper motor to precisely control the traveling of the flame over the distance of few centimeters. When the tapering process begins, the pulling motors move outward to pull the heated fiber and the flame simultaneously starts to travel back-and-forth for heating the region to be tapered. The pulling mechanism employs a high-precision stepping motor with a right-and-left-threaded screw to drive two V-groove clampers moving outward in a reverse direction. The clampers bilaterally hold the single-mode fiber for providing a precise pulling stress. By controlling the moving speed of the scanning flame and the pulling clampers, the total elongation length can be varied from 30 to 60 mm, and the corresponding length of the uniform waist is measured to be around 10–25 mm, contingent on the waist diameter. When

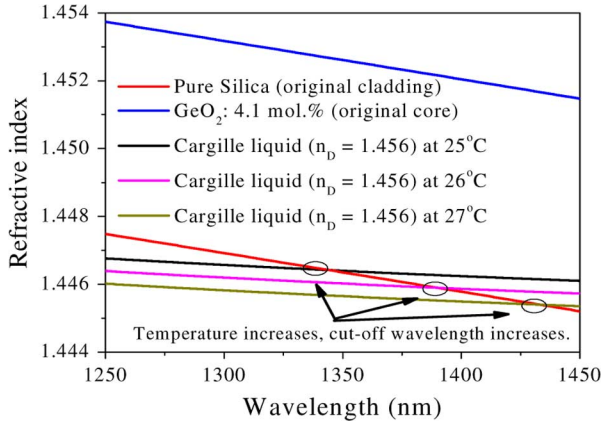

Fig. 2. Material dispersion curves for the original fiber core (GeO2 4.1 mol%), cladding (pure silica), and the index-matching liquids measured at 25, 26, and 27°C, respectively.

tapering is finished, the fiber is fixed in a graved U-groove on a quartz substrate and immersed in index-matching liquids. A TE cooler is used to control the liquid temperature to change its refractive index for tuning the cutoff wavelength.

When a single-mode optical fiber is tapered down to few tens micrometer in diameter, the evanescent tail of the mode field spreads out of the fiber cladding and reaches the external environment (Cargille liquids). The size of the Ge-doped core in the tapered zone is so reduced that its waveguiding effects are negligible. Therefore, the pure silica cladding plays as the new core, whereas the external medium serves as the new cladding. The material dispersion curves for the original fiber core (GeO2 4.1 mol%), cladding (pure silica), and the Cargille liquids are plotted in Fig. 2 to illustrate their relative relation. On the right-hand side of the cross point indicated in Fig. 2, the refractive index of the liquids is greater than the index of fiber taper and the total internal reflection of the interface is frustrated. Therefore, the lights cannot be guided in the fiber taper and suffer a great amount of optical loss. On the other hand, the light can be nicely confined in the fiber taper when the wavelength is shorter than the cutoff wavelength. The cutoff wavelength of the short-wavelength-pass filter should be very near the cross point of the two dispersion curves indicated in Fig. 2, under the condition that the mode in the tapered region is mainly guided by the original cladding. The temperature shift of the cross point as also indicated in Fig. 2 provides an intuitive explanation about the temperature-tuning capability of the tapered-fiber filter.

It should also be noted that a related but different kind of short-wavelength-pass optical filtering effects can be observed when the tapered fiber waist is in the 100 nm range. [17] The tapered fiber is surrounded by the air, and an abrupt change of the mode field diameter as a function of the optical wavelength can be found. This leads to an abrupt change of optical loss accordingly. However, since no dispersion engineering is used to produce true optical cutoff, the filtering slope and rejection ratio are not as large as the cutoff case studied here.

III. Experimental and Simulation Results

Both the experimental and simulated spectral responses of the short-wavelength-pass fiber are displayed in Fig. 3 for perfor-

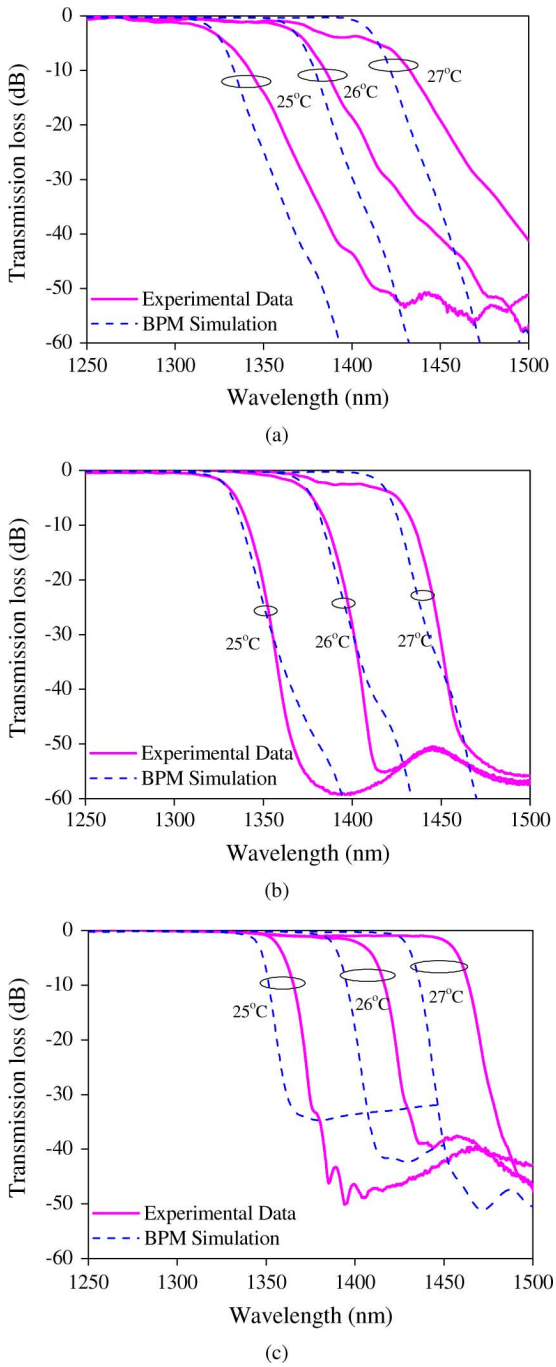

Fig. 3. Experimental and simulated spectral responses of the tunable short-wavelength-pass fiber filters for (a) $\rho = 20\ \mu$m, (b) $\rho = 26\ \mu$m, and (c) $\rho = 40\ \mu$m at different temperatures.

mance studies and comparison. The solid lines of Fig. 3(a)–(c) display the experimental spectral responses of the short-wavelength-pass filter with waist diameters measured to be 20, 26, and 40 μm, respectively. The total elongation lengths are about 30 mm, and the lengths of the uniform waist are measured to be around 18 mm. The larger the waist diameter is, the steeper the cutoff slope can be. Here the cutoff slope (in unit: dB/nm) is defined as the average gradient of the rolloff spectral curve in the linear region from -10 to -30 dB transmission loss. The cutoff slopes are calculated to be -0.54, -1.38, and -2.00 for the cases of $\rho = 20\ \mu$m, $\rho = 26\ \mu$m, and $\rho = 40\ \mu$m, respectively. When $\rho = 40\ \mu$m, the cutoff slope is very sharp, but the rejection efficiency is more limited. The extra loss of less than 2 dB at 1390 nm may result from the absorption of hydroxyl ions which were generated from the hydrogen flame and then diffused into the tapered fiber. The tuning efficiencies of the filter are about 52, 47, and 62 nm/°C for the cases of $\rho = 20\ \mu$m, $\rho = 26\ \mu$m, and $\rho = 40\ \mu$m, respectively. At the guiding wavelengths, the insertion losses of the filters are below 1 dB, 0.5 dB, and 0.3 dB for $\rho = 20\ \mu$m, $\rho = 26\ \mu$m, and $\rho = 40\ \mu$m, respectively. The losses are mainly from the absorption loss of the Cargille liquids and the optical loss due to fiber tapering. The absorption loss caused by the Cargille liquids is estimated to be below 0.2 dB after taking into account the transmittance of the liquids and the evanescent field overlapping effects. The fiber-tapering loss depends on the tapering conditions. In principle, when the tapering transition is slow enough to meet the adiabatic criteria [18], the tapering loss can be made very small. For our cases, the tapering loss is reasonably low but still observable, as can be seen from the above numbers. Even smaller tapering losses should be possible at the cost of increasing the total device length.

To further analyze the fundamental-mode cutoff characteristics, numerical simulation by the BPM is performed to study the optical field propagation within the tapered fibers and to predict the filter performance theoretically. The BPM uses the finite difference method to solve the paraxial approximation of the Helmholtz equation with "transparent" boundary conditions [19]. This approach can automatically include the effects of all the guided and radiation modes as well as the mode-coupling and mode-conversion effects. The fiber-taper transition structure is set to be an exponential shape in our simulation. The dotted lines in Fig. 3(a)–(c) show the simulated transmission spectra with the temperatures of 25, 26, and 27°C and the waist diameters of 20, 26, and 40 μm, respectively. The cutoff wavelengths gradually shift to longer wavelengths when the temperature increases. Good agreement of the changing trends for the cutoff slopes and rejection efficiencies between the simulated and experimental results has been found. The mismatch of the cutoff wavelengths between the experimental data and simulation results should be due to the uncertainties of the fiber-tapering parameters and the temperature-reading errors in the experiment. Most importantly, the simulation results correctly reproduce the experimental observation that the larger diameter cases have larger cutoff slopes, but will eventually have poorer rejection ratios when ρ is too large ($> 40\ \mu$m). The thermo-optic-tuning efficiency of the filter for $\rho = 26\ \mu$m in Fig. 3(b) is about 48 nm/°C from BPM simulation, which is also in good agreement with the 47 nm/°C tuning efficiency from the experimental data.

Based on the facts that the theoretically predicted tuning and cutoff efficiencies agree reasonably with the experimental data, we further utilize the BPM as a reliable simulation tool to investigate the effects of different taper parameters for determining the optimal taper structures.

Fig. 4(a) and (b) show the simulated field evolution within a tapered fiber with the cutoff wavelength around 1330 nm. The waist diameter ρ is 26 μm, the transition length τ is 6 mm, the

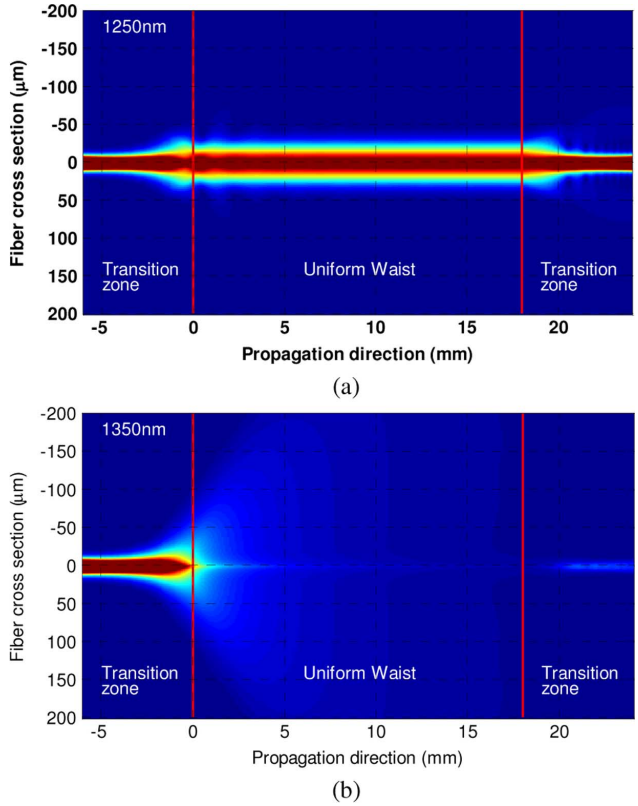

Fig. 4. Field distributions along the tapered-fiber filter. (a) When the wavelength (1250 nm) is shorter than the band edge of the filter, the fields are guided over uniform waist and coupled back to the fundamental mode. (b) When the wavelength (1350 nm) is longer than the band edge of the filter, the fields spread out along the uniform waist.

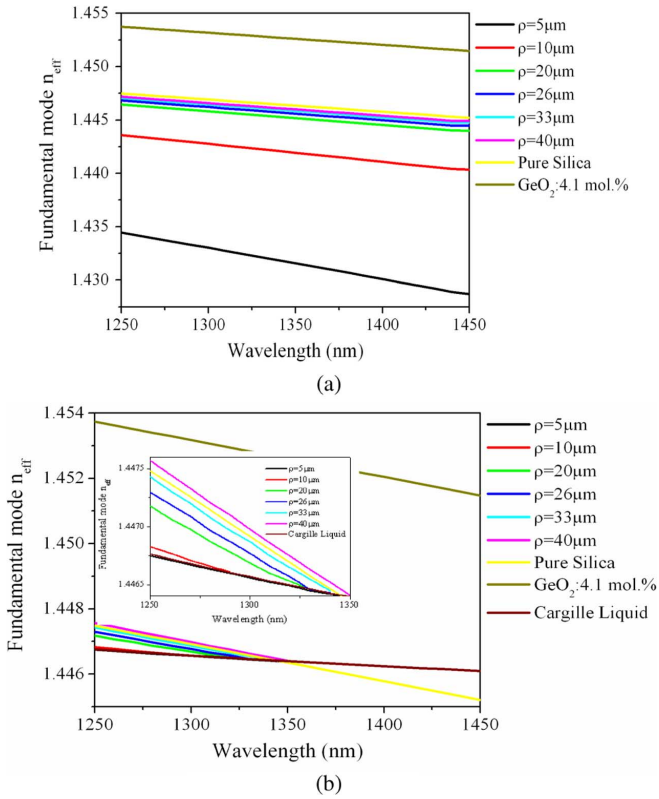

Fig. 5. (a) Effective index of the fundamental mode versus wavelength under different waist diameters of tapered fibers surrounded by (a) the air, and (b) the Cargille liquids ($n_{\mathrm{D}} = 1.456$).

taper transition angle is around 0.5°, the uniform waist length L_0 is 18 mm, and the temperature is set at 25°C. In Fig. 4(a), when the propagation wavelength (1250 nm) is shorter than the cutoff wavelength, the fundamental eigenmode of the input SMF is smoothly transformed into the fundamental eigenmode of the uniform tapered waist, propagates through the uniform waist region and then gradually reconverts to the fundamental mode of the output SMF within the second transition distance τ. The fundamental MFD is larger in the uniform tapered region when compared to that of the SMF-28. On the other hand, Fig. 4(b) shows the case when the propagation wavelength (now 1350 nm) is longer than the cutoff wavelength. The optical field quickly disperses away within the first taper transition region as well as the uniform waist region due to the higher refractive index of the surrounding liquids. Only a very small fraction of the optical field can be coupled back to the fundamental mode of the output SMF. In this way, huge optical losses are induced for wavelengths longer than the cutoff wavelength.

The material dispersion of the surrounding medium can significantly modifies the dispersion curve of the propagation mode due to the stronger overlap with the evanescent field spread out of the taper waist. To analyze how the surrounding material affects the dispersion properties of the fused-tapered fiber, the effective index of fundamental mode is calculated under different waist diameters of tapered fibers surrounded by the air and the Cargille liquids ($n_{\mathrm{D}} = 1.456$). The results are plotted in Fig. 5(a) and (b). The material dispersion curves of the original Ge-doped core, the cladding (pure silica), and the Cargille liquids are also plotted for easy comparison. The index difference of the pure silica and the air is so large that the optical field is strongly confined when the tapered fiber is surrounded by the air. Thus, the dispersion curves of the fundamental mode have almost the same slope ($dn_{\mathrm{eff}}/d\lambda = -1.2 \times 10^{-5}$/nm) with that of the pure silica when $\rho > 20\ \mu$m. The effective mode index is lower than those of the pure silica and Ge-doped core because parts of the optical mode field are now in the air. When the waist diameter gets smaller than 5 μm, the dispersion curve of the fundamental mode becomes more wavelength dependent. This is because now a larger fraction of the mode field is in the air. The slopes of the dispersion curves in Fig. 5(b) are calculated to be $-0.55 \times 10^{-5}, -0.87 \times 10^{-5}, -0.94 \times 10^{-5}, -1.07 \times 10^{-5}$, and -1.14×10^{-5} for $\rho = 10\ \mu$m, $\rho = 20\ \mu$m, $\rho = 26\ \mu$m, $\rho = 33\ \mu$m, and $\rho = 40\ \mu$m, respectively. In contrast, the slopes of the modal dispersion curves for tapered fibers immersed in the Cargille liquids are slightly flatter than those in the air, which indicates that the effective mode index of the tapered fiber is indeed modified by the surrounding dispersive liquids. The insect of Fig. 5(b) shows the detailed curves near the cutoff wavelength when the tapered fibers are immersed in the Cargille liquids. The cross points between the dispersion curves of the tapered fibers and the surrounding liquids exactly determine the cutoff wavelength, which will shift to longer wavelengths as the waist diameter increases. When the optical wavelength is near the cross point, the optical field quickly spreads out of the tapered fibers

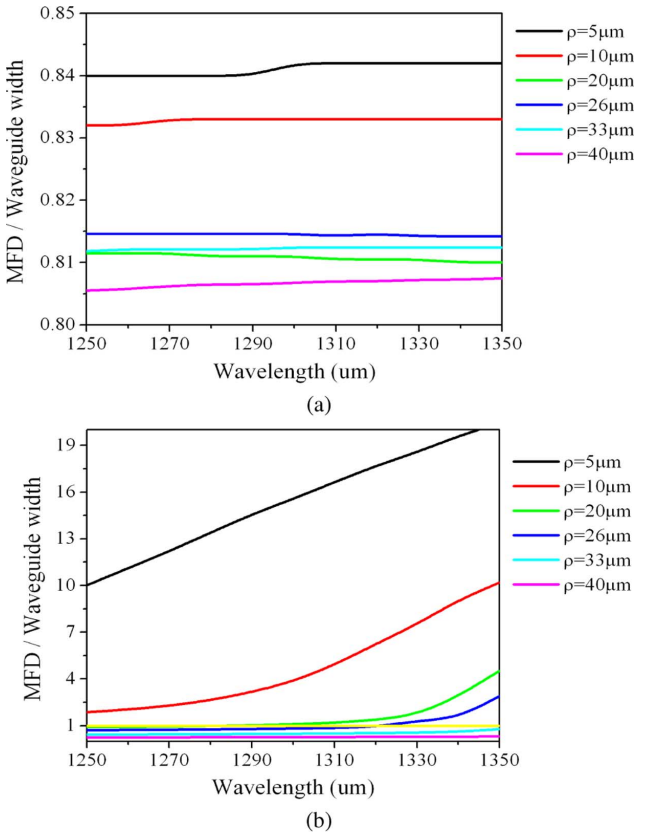

Fig. 6. MFD/waveguide width versus wavelength under different waist diameters of tapered fibers surrounded by (a) the air, and (b) Cargille liquids ($n_{\mathrm{D}} = 1.456$).

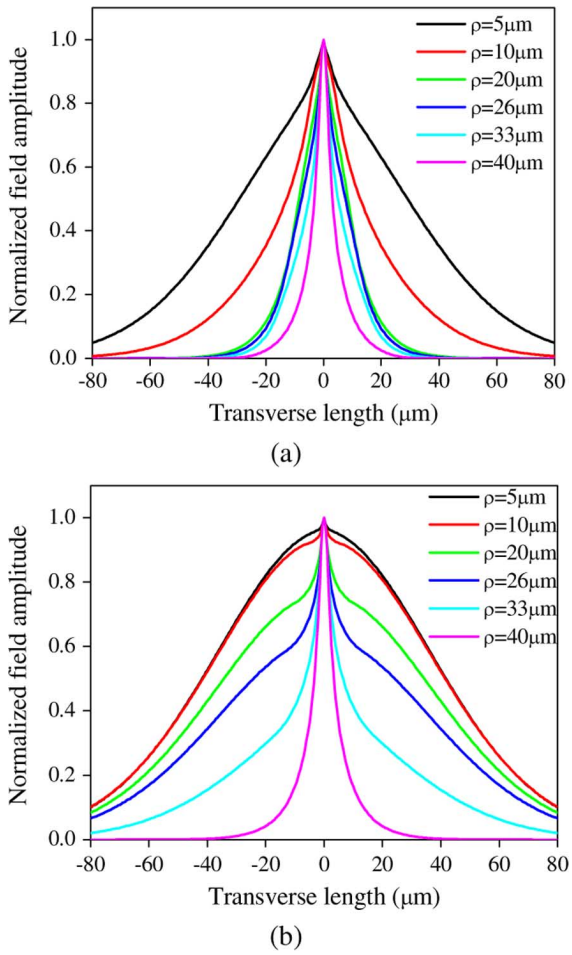

Fig. 7. Fundamental-mode-field distribution in the tapered waist under different taper diameters at (a) 1250 nm (guiding wavelength) and (b) 1350 nm (near cutoff wavelength).

and large optical losses are induced. Intuitively the cross angle between the two intersected dispersion curves determines the cutoff slope. A suitable surrounding material which can produce a larger intersection angle is thus a key for achieving high-cutoff efficiency.

Fig. 6(a) and (b) plot the ratio of the 1/*e* MFD to the waveguide width (waist diameter of the tapered fiber) as a function of the optical wavelength. When the tapered fiber is surrounded by the air, the optical field is strongly confined inside the tapered fiber and thus the width ratio is almost flat with respect to the optical wavelength for the waist diameters considered here. In contrast from Fig. 6(b) it is obvious that a larger fraction of the optical field spreads out of the tapered fiber when it is surrounded by the Cargille liquids due to the small index difference. As the waist diameter is getting smaller, the width ratio gets larger. When the waist diameter is smaller than 10 μm, the optical fields will largely spread out of the tapered waveguide region and will experience higher losses even at guided wavelengths. When the waist diameter is between 20 μm and 26 μm, the width ratio curves exhibit a significant turning point between the guided region and the unguided region, as shown in Fig. 6(b). When the waist diameter is larger than 40 μm, the cutoff wavelength is shifted toward the longer wavelengths, and the optical field is more strongly confined in the waveguide. The dispersion-engineered effects can also be seen from the wavelength dependence of the MFD. Fig. 7(a) and (b) show the mode field distribution of the fundamental mode in the tapered waist under different taper diameters. Two optical wavelengths at 1250 nm (guiding) and 1350 nm (near cutoff) are used as the examples to illustrate the difference. The field is strongly confined in the tapered region for the guiding wavelengths when $\rho > 20$ μm. As the waist diameter gets smaller than 10 μm, the field spreads out of the tapered fiber region and larger losses at the guiding wavelengths are produced. Near the cutoff wavelength in Fig. 7(b), the field extends more widely into the Cargille liquids due to the weak guiding condition. Thus, the loss becomes huge and the short-wavelength-pass band edge is formed. Moreover, the larger taper diameters ($\rho > 33$ μm) can confine the fields more tightly than the smaller ones even near the cutoff wavelength.

Fig. 8 shows the simulated transmission spectra of the fiber taper with the waist diameter of 5, 10, 20, 26, 33, 45, and 60 μm, respectively. The fiber transition length τ is 6 mm, the uniform waist length L_0 is 18 mm, and the temperature is at 25°C. The spectral cutoff responses are not the same for different waist diameters. Note that as the waist diameter increases, the band edge is steeper. The cutoff slopes are calculated to be $-0.38, -0.79, -1.14, -1.68$, and -2.01 for $\rho = 10$ μm, $\rho = 20$ μm, $\rho = 26$ μm, $\rho = 33$ μm, and $\rho = 40$ μm, respectively. The band-edge shifts to the longer wavelengths as the diameter increases. The cutoff characteristics in Fig. 8 can be

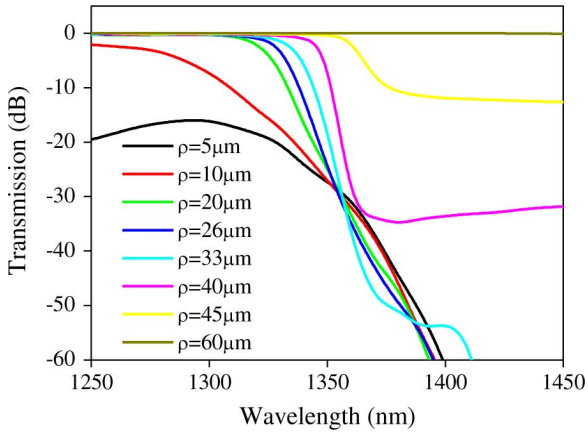

Fig. 8. Simulation results of transmission spectra at different waist diameters of 5, 10, 20, 26, 33, and 40 μm, respectively.

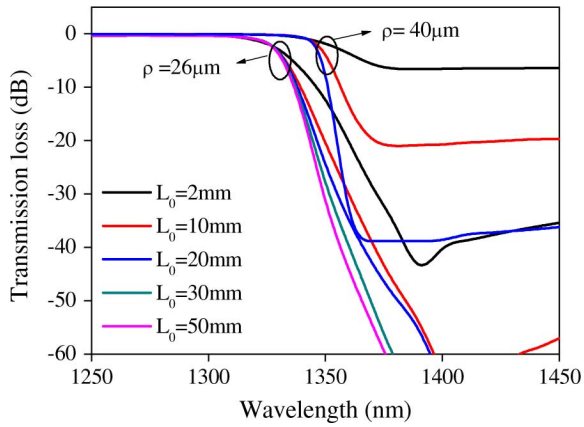

Fig. 9. Transmission spectra associated with different lengths of uniform waist of 2 mm, 10 mm, 20 mm, 30 mm, and 50 mm for $\rho = 26$ μm and 2 mm, 10 mm, 20 mm for $\rho = 40$ μm with the taper transition length of 6 mm.

TABLE I
THE CUTOFF SLOPES AND DISPERSION SLOPES FOR DIFFERENT WAIST DIAMETERS OF TAPER FILTERS IMMERSED IN CARGILLE LIQUID

Taper diameter	Dispersion slope Δn_{eff} / nm ($\times 10^{-5}$)	Cutoff slope dB / nm	
10 μm	-0.55	-0.38(simulation)	
20 μm	-0.87	-0.79(simulation),	-0.54(experimental)
26 μm	-0.94	-1.14(simulation),	-1.38(experimental)
33 μm	-1.07	-1.68(simulation)	
40 μm	-1.14	-2.01(simulation),	-2.00(experimental)

described by the waveguide dispersion behavior with different waist diameters. The optical field intensely spreads out into the Cargille liquids when the waist diameter is getting small. The ratio of the optical field distributed in the waveguide with respect to that in the Cargille liquids is strongly decisive to the effective index of the mode field. When the diameter is less than 10 μm, the waist is too thin to confine the optical field. Furthermore, when the waist diameter is getting thinner, most optical field extends into the Cargille liquids, the wave-guiding ability is weaker, and thus the transmission loss becomes larger. The simulation results indicate that the larger the waist diameter is, the steeper the filter cutoff slope can be. However, when the waist diameter is larger than 40 μm, the achievable spectral contrast (or rejection efficiency) is more limited due to the stronger mode confinement. The short-wavelength-pass bend edge disappears when the tapered waist is larger than 60 μm. All the wavelengths are now strongly confined in the Ge-doped fiber core. Thus, the optimal waist diameter for fused-tapered SMFs to produce a sharp short-wavelength-pass band edge should be somewhere between 33 μm and 40 μm.

Table I lists the cutoff slopes and dispersion slopes for the waist diameters of 5, 10, 20, 26, 33, and 40 μm, respectively. When the waist diameter is larger, the dispersion slopes are larger and the cutoff slopes are steeper. It also can be clearly seen that steeper cutoff slopes are associated with larger cross angles between the dispersion curves of the tapered fibers and the surrounding liquids. The good agreement of the cutoff slopes from experimental and simulated results confirms that the simulation can help predict the filter performance.

Fig. 9 indicates that the length of the uniform waist also has certain influences on the cutoff slope of the filter's band edge. The simulation is performed under the assumption that the temperature is 25°C, the fiber taper waist diameter and the waist length are $\rho = 26$ and 40 μm, respectively, and the transition length is $\tau = 6$ mm. The tapers have the waist length of 2, 10, 20, 30, and 50 mm for $\rho = 26$ μm and the waist length of 2, 10, 20 mm for $\rho = 40$ μm, respectively. It can be seen that the longer length leads to a steeper band edge for $\rho = 26$ μm. When the waist length is shorter than 30 mm, the cutoff slopes of the band edge significantly increase with the waist length. Since the optical loss is proportional to the taper length, it is not surprised that longer taper length causes higher cutoff loss and thus provides a sharper cutoff slope. However, when the waist length is longer than 30 mm, the cutoff slopes become saturated. For $\rho = 40$ μm, the length of the uniform waist not only influences the cutoff slopes but also affects the rejection efficiencies. The rejection efficiency relies on the sufficient cutoff loss of long taper length. At $\rho = 40$ μm, the optical field is more confined in the tapered waist, and thus the optical cutoff loss is more limited. Since the simulation results indicate that the longer the taper length is, the steeper the filter cutoff slope can be, the optimal waist length for fused-tapered SMF-28 should be at least larger than 20 mm.

To further investigate how the waveguide structure influences the cutoff slopes and optical losses, the taper transition length is varied from 3 mm (taper transition angle around 1.0°), 6 mm (taper transition angle around 0.5°), to 12 mm (taper transition angle around 0.2°). The tapered fiber has a fiber taper waist diameter $\rho = 26$ um and the waist length $L_0 = 18$ mm. The obtained spectral responses are shown in Fig. 10. The smaller filter transmission losses in the shorter wavelength side indicate that longer taper transition length can more guarantee low-loss conversion from the SMF-28 region to the taper region. At guiding wavelengths, the insertion loss of the filter is below 1.1 dB, 0.3 dB, and 0.01 dB for the cases of $\tau = 3$ mm, 6 mm, and 12 mm. The loss difference for guided wavelengths can be as high as 1 dB between $\tau = 3$ and $\tau = 12$ mm. The optimal design of the ratio between the taper transition length to the taper diameter should be at least larger than 6 mm/26 μm (i.e., the

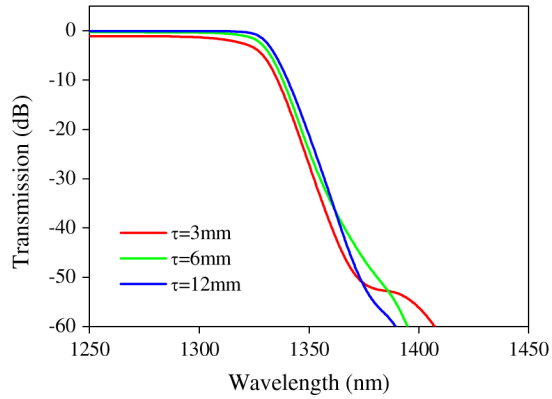

Fig. 10. Transmission spectra associated with different transition lengths of 3 mm, 6 mm, and 12 mm with the waist length of 18 mm for $\rho = 26\ \mu$m.

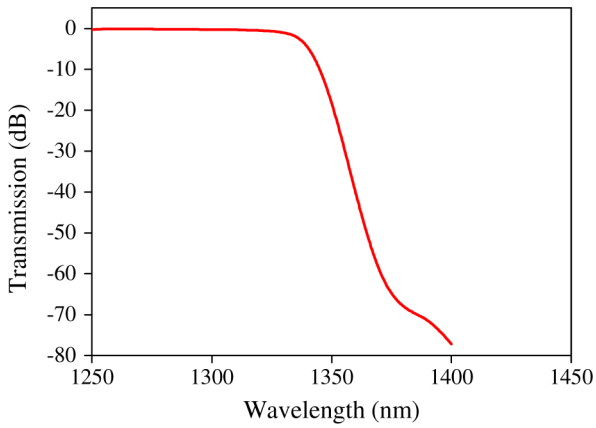

Fig. 11. Transmission spectra of the final optimal design of the short-wavelength-pass filter. The taper waist diameter is 35 μm, the waist length is 30 mm, and the transition length is 6 mm.

transition angle of the fiber structure should be less than 0.5°). Based on the above theoretical analyses, the optimal design parameters for the taper waist diameter, waist length, and transition length should be somewhere around 26–40 μm, 30 mm, and 6 mm, respectively.

As the final verification, we set the taper waist diameter, waist length, and transition length to be 35 μm, 30 mm, and 6 mm, respectively, and perform the BPM simulation. The calculated spectral response is shown in Fig. 11. The rejection efficiency is as high as 70 dB, the cutoff slope is as high as -2.4 dB/nm, and the insertion loss is less than 0.3 dB. These results indicate the performance improvement that can be expected by carefully adjusting the device parameters.

The aim of this work is based on one of our previous experimental works [9] to investigate the influences of the taper length, taper diameter, and transition length on the spectral cutoff slope and rejection ratio of the tapered-fiber filter. The optimization is not absolute in the sense that additional constrains need to be considered. For example, the total length of the device cannot be too long for the ease of practical fabrication. Through this kind of optimization, we can know how much performance improvement can be expected by practically adjusting the device parameters. The Cargille liquids provide a cost-effective, simple, and fast way to implement the fundamental-mode cutoff mechanism. In principle, there should be many other optical materials such as optical glass or optical polymers that can be employed to realize short-pass filters for practical applications. [20] This will be one of the directions for our future studies.

IV. Conclusion

In summary, a new type of thermo-optic tunable short-wavelength-pass fiber filters based on fiber tapering and dispersion engineering has been demonstrated experimentally and analyzed theoretically. Good agreements between the BPM simulation and experimental results are achieved. The effects of material dispersion and waveguide dispersion characteristics have been investigated by examining the spectral response as well as the changing trends of the MFD and the effective mode index. An optimized tapered fiber filter structure that can attain high-cutoff efficiency has been suggested based on the obtained theoretical simulation results. We find for SMF-28 raw fibers, the uniform tapered waist diameter should be around 35 μm, the uniform tapered-waist length should be greater than 30 mm, and the tapered-transition length should be greater than 6 mm. With such an optimized structure, the cutoff slope can be as high as -2.4 dB/nm, the rejection efficiency can be as high as 70 dB, and the fundamental mode-coupling loss is below 0.3 dB. In principle, if different choices of raw fibers can be used, it is possible that the performance can be even more optimized. The analyses presented in the present work should be helpful for developing inline tapered fiber filters based on the dispersion-engineered fundamental-mode cutoff mechanism.

Acknowledgment

The authors thank Prof. Chii-Chang Chen of Department of Optics and Photonics, National Central University, Taiwan, for his kindly help on simulation. This research is partially supported by the National Science Council of the Republic of China (NSC 96-2221-E-009-128-MY3), the MOE ATU program of National Chiao Tung University (MOE ATU program), and Center for Measurement Standards, Industrial Technology Research Institute.

References

[1] W. Ding and S. R. Andrews, "Modal coupling in surface-corrugated long-period-grating fiber tapers," *Opt. Lett.*, vol. 33, no. 7, pp. 717–719, 2008.

[2] Y. Li and L. Tong, "Mach-Zehnder interferometers assembled with optical microfibers or nanofibers," *Opt. Lett.*, vol. 33, no. 4, pp. 303–305, 2008.

[3] J. Lou, L. Tong, and Z. Ye, "Dispersion shifts in optical nanowires with thin dielectric coatings," *Opt. Express*, vol. 14, no. 16, pp. 6993–6998, 2006.

[4] C. M. B. Cordeiro, W. J. Wadsworth, T. A. Birks, and P. St. J. Russell, "Engineering the dispersion of tapered fibers for supercontinuum generation with a 1064 nm pump laser," *Opt. Lett.*, vol. 30, no. 15, pp. 1980–1982, 2005.

[5] J. Villatoro, D. Monzón-Hernández, and D. Luna-Moreno, "In-line tunable band-edge filter based on a single-mode tapered fiber coated with a dispersive material," *IEEE Photon. Technol. Lett.*, vol. 17, no. 8, pp. 1665–1667, Aug. 2005.

[6] F. Warken, E. Vetsch, D. Meschede, M. Sokolowski, and A. Rauschenbeutel, "Ultra-sensitive surface absorption spectroscopy using sub-wavelength diameter optical fibers," *Opt. Express*, vol. 15, no. 19, pp. 11952–11958, 2007.

[7] G. Brambilla, G. Senthil Murugan, J. S. Wilkinson, and D. J. Richardson, "Optical manipulation of microspheres along a subwavelength optical wire," *Opt. Lett.*, vol. 32, no. 20, pp. 3041–3043, 2007.
[8] N. K. Chen, S. Chi, and S. M. Tseng, "Wideband tunable fiber short-pass filter based on side-polished fiber with dispersive polymer overlay," *Opt. Lett.*, vol. 29, no. 19, pp. 2219–2221, 2004.
[9] N. K. Chen, K. C. Hsu, S. Chi, and Y. Lai, "Tunable Er^{3+}-doped fiber amplifiers covering S and C + L bands over 1490–1610 nm based on discrete fundamental-mode cutoff filters," *Opt. Lett.*, vol. 31, no. 19, pp. 2842–2844, 2006.
[10] N. K. Chen, C. M. Hung, S. Chi, and Y. Lai, "Towards the short-wavelength limit lasing at 1450 nm over ${}^4I_{13/2} \rightarrow {}^4 I_{15/2}$ transition in silica-based erbium-doped fiber," *Opt. Express*, vol. 15, no. 25, pp. 16448–16456, 2007.
[11] C. M. Hung, N. K. Chen, Y. Lai, and S. Chi, "Double-pass high-gain low-noise EDFA over S-and C+L-bands by tunable fundamental-mode leakage loss," *Opt. Express*, vol. 15, no. 4, pp. 1454–1460, 2007.
[12] T. Birks and Y. Li, "The shape of fiber tapers," *J. Lightw. Technol.*, vol. 10, no. 4, pp. 432–438, 1992.
[13] S. Xue, A. van Eijkelenborg, G. W. Barton, and P. Hambley, "Theoretical, numerical, and experimental analysis of optical fiber tapering," *J. Lightw. Technol.*, vol. 25, no. 4, pp. 1169–1176, 2007.
[14] M. Sumetsky, "How thin can a microfiber be and still guide light?," *Opt. Lett.*, vol. 31, no. 7, pp. 870–872, 2006.
[15] M. Sumetsky, "Optics of tunneling from adiabatic nanotapers," *Opt. Lett.*, vol. 31, no. 23, pp. 3420–3422, 2006.
[16] R. Zhang, X. Zhang, D. Meiser, and H. Giessen, "Mode and group velocity dispersion evolution in the tapered region of a single-mode tapered fiber," *Opt. Express*, vol. 12, no. 24, pp. 5840–5848, 2007.
[17] M. Sumetsky, Y. Dulashko, P. Domachuk, and B. J. Eggleton, "Thinnest optical waveguide: Experimental test," *Opt. Lett.*, vol. 32, no. 7, pp. 754–7562, 2007.
[18] J. D. Love, W. M. Henry, W. J. Black, S. Lacroix, and F. Gonthier, "Tapered Single-mode Fibres and Devices Part 1: Adiabaticity criteria," *IEE Proc. J.*, vol. 138, no. 5, pp. 343–354, 1991.
[19] R. Scarmozzino and R. M. Osgood, Jr., "Comparison of finite-difference and Fourier-transform solutions of the parabolic wave equation with emphasis on integrated-optics applications," *J. Opt. Soc. Amer. A*, vol. 8, no. 5, pp. 724–731, 1991.
[20] N. K. Chen, S. Chi, and S. M. Tseng, "Wideband tunable fiber short-pass filter based on side-polished fiber with dispersive polymer overlay," *Opt. Lett.*, vol. 29, no. 19, pp. 2219–2221, 2004.

Sen-Yih Chou was born in 1971. He received the B.S. and M.S. degrees from the Department of physics, National Sun Yat-sen University, Taiwan, in 1994 and 1996, respectively.

He was an R&D engineer in Materials and Electro-optics Research Division in Chung-Shan Institute of Science & Technology from 1998 to 2000. From June 2006 to date, he was an R&D engineer in Center for Measurement Standards in industrial technology Research Institute.

He is progressing Ph.D. program in the Department of Photonics, National Chiao Tung University, Taiwan, from August 2002 to date.

Kuei-Chu Hsu was born in 1974. She received the Ph.D. degree from the National Chiao-Tung University, Taiwan, in 2007.

She is a Postdoctoral Research Fellow with the Department of Photonics, National Chiao Tung University, Taiwan. Her research interests include fiber sensors and fiber lasers, photonic crystal devices, and liquid crystal optics.

Nan-Kuang Chen was born in 1973. He received the B.Sc. and M.Eng. degrees from National Tsing Hua University, Taiwan, in 1996 and 1998, respectively, the Ph.D. degree from National Chiao Tung University, Taiwan, in 2006.

In August 2007, he joined the Department of Electro-Optical Engineering, National United University, Taiwan. He is currently an Assistant Professor and the Director of Optoelectronics Research Center. Dr. Chen has authored and co-authored over 35 international SCI journal articles and conference presentations. His research interests include dispersion engineering, fiber-integrated devices, biophotonic sensors, and high power fiber lasers.

Dr. Chen is a member of OSA and IEEE LEOS.

Shien-Kuei Liaw (M'00) was born in 1965. He received the BSEE, MSEE and Ph.D. degrees from the National Taiwan University, National Tsing-Hwa University and National Chiao-Tung University, Taiwan, in 1988, 1993 and 1999, respectively.

In 1993, he joined the Telecommunication Laboratories, Ministry of Transportation and Communications, Taiwan. Since then, he has been working on fiber optics communication and fiber based devices. In 1996, he was a visiting scholar at Bellcore (now Telcordia), Red Bank, NJ. He is currently a Full Professor and Deputy Director of Optoelectronics Center at the National Taiwan University of Science and Technology, Taiwan. He has authored and co-authored over 110 international journal articles and conference presentations. His research interests include WDM transmission, fiber devices, and fiber-optic sensing systems. Dr. Liaw is a member of IEEE LEOS, SPIE and OSA.

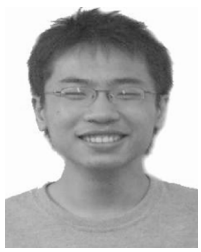

Yu-Syun Chih was born in 1985. He received the B.S. degrees from National Changhua University of Education, Taiwan, in 2007. He is a master student with Department of Photonics, National Chiao Tung University, Taiwan. Yu-Syun Chih has co-authored two international SCI journal articles.

His research is currently focused on optical fiber devices such as fiber-filter and fiber -sensor.